Scaling behavior of the tensile strength of viscocohesive granular aggregates

Thanh-Trung Vo *

Bridge and Road Department, Danang Architecture University, 550000 Da Nang City, Vietnam

(Received 28 December 2020; accepted 22 March 2021; published 12 April 2021)

We numerically analyze the tensile strength of a single wet agglomerate modeled as a viscocohesive aggregate impacting a flat surface by using the discrete-element simulations. The viscocohesive agglomerate composed of primary spherical particles with the inclusion of the interstitial liquid in the form of the capillary bridges characterized by the cohesive and viscous forces between particles is extracted from a cuboidal sample of granular materials by applying a spherical probe. The tensile strength is measured from the impact test of a wet agglomerate by systematically varying different values of the surface tension of the interstitial liquid, the liquid viscosity, and the impact speed. We show that the tensile stress increases immediately when the collision occurs between the agglomerate and the flat surface. The peak of the tensile stress obtained after the collision, then decreases smoothly with increasing the particle movement. The maximum tensile stress is defined to be the tensile strength of such agglomerate. It is remarkable that the normalized tensile strength of such agglomerate can be well described as a function of a dimensionless impact number that incorporates the capillary number and Stokes number (calculated from the surface tension and the viscosity of the liquid and the impact rate of the agglomerate), thus providing the confirmation for the unified representation of the liquid properties and the impact rate of wet granular media.

DOI: 10.1103/PhysRevE.103.042902

I. INTRODUCTION

Wet aggregates, viscocohesive aggregates, or cemented aggregates commonly appear in nature and industrial processes [1–6]. Important components of aggregates involve raw materials and interstitial liquid which are presented in the structure of the capillary bridges between grains [6–12]. These capillary bridges are the consequence of the condensation of the liquid vapor or drainage in the nature and the mixing of the binding liquid and the particles in the industry [13–18]. The liquid commonly induces the cohesive forces and the viscous forces between particles [18,19]. These forces increase the mechanical strength of viscocohesive agglomerates [4,17]. Besides the compressive stress that is nearly understood based on previous studies over the last few decades, the tensile strength of such agglomerates needs further investigation, especially when considering both cohesive and viscous interactions between grains.

In order to study the tensile strength of wet granular materials, here we consider the case in which an agglomerate impacts on a rigid surface by setting its initial position and initial velocity applied for all primary particles. At the beginning of the collision process, the aggregate receives the external forces from the rigid plane and transmits them to the agglomerate based on the interactions between primary particles. These interactions involve the elastic and frictional forces, and the cohesive and viscous forces which depend on the properties of the binding liquid. Meanwhile, the cohesive forces only represent the contractive properties between spherical particles; the viscous forces mobilize in the direction of the extension or contraction depending on the relative movement between particles which may depend on the impact speed and microstructure of agglomerates [20]. Thus, it is necessary to get a better understanding of the effects of the cohesive and viscous interactions as well as the impact rate on the tensile strength of viscocohesive agglomerates.

Actually, the effects of liquid properties characterized by the cohesive and viscous forces between particles and the flow rate of granular materials are previously investigated in terms of the rheology of steady-state shearing flows and the evolution of agglomerates in different configurations and environments [6,12,17,19,21–23]. In the viscoinertial simple shear flows of granular materials, the effective friction coefficient and the packing fraction can be described as a function of a dimensionless number combining the particle inertia and the liquid viscosity [20,24–26]. In the steady-state simple shear flows of cohesive material, the combination of the particle inertia and the cohesive forces could scale its rheological properties [17,27]. In particular, when both cohesive and viscous effects come into play with the frictional and elastic interactions between particles, the rheology of unsaturated granular flows and the erosion rate of wet particle agglomerates can be scaled as a function of a dimensionless number which incorporates the particle inertia, cohesive stress, and viscous stress [18,19]. These above examples raise the question whether the tensile strength of wet agglomerates generated in the impact test can also be scaled as a function of a new dimensionless number incorporating the liquid-vapor surface tension, the liquid viscosity, and the impact rate. This will be nontrivially addressed in this current paper.

In this paper, we analyze the tensile strength of viscocohesive agglomerates impacting a flat surface by means of three-dimensional (3D) numerical simulations. The

*trungvt@dau.edu.vn

 ©2021 American Physical Society

simulations were carried out by means of the discrete-element method with the inclusion of the viscous and cohesive forces of the binding liquid. The agglomerates are extracted from a cuboidal sample of viscocohesive granular materials. By systematically varying broad ranges of values of the liquid viscosity and the surface tension of the interstitial liquid as well as the impact speed as setting different values of the initial velocity of the agglomerate, we investigate the tensile stress of such aggregate. This tensile stress increases proportionally to the system parameters above, and as we shall see, the tensile strength of a viscocohesive aggregate can be nontrivially behaved by a dimensionless impact number incorporating all key parameters.

In the following, we introduce the sample preparation and parameters used to prepare the impact test of agglomerates in Sec. II. In Sec. III, we discuss the evolution of the tensile stress as a function of the particle displacement for different values of the system parameters. Then, we propose the scaling behavior of the tensile strength in Sec. IV. We conclude in Sec. V with the summary of the salient results and further research directions. We briefly introduce the numerical method in the Appendix.

II. MODEL SETTING AND PARAMETERS

The viscocohesive agglomerate composed of 31 470 spherical particles was first prepared by introducing a cuboidal sample of spherical particles under an isotropic compaction. The particle diameter is varied in a range $[d_{\min}, d_{\max}]$ with $d_{\max} = 2 \times d_{\min}$. After the cuboidal sample of spherical particles reaches the equilibrium state, we added the interstitial liquid characterized by the cohesive and viscous forces between particles, and the liquid is assumed to be homogeneously distributed inside the sample. Then, we placed in the center of the cuboidal sample a spherical probe in order to extract the agglomerate. Finally, this agglomerate is allowed to reach the relaxation under the action of both cohesive and viscous forces. These forces are shown in the Appendix below.

The viscocohesive agglomerate is then subjected to the impact test by setting its initial position having the height equal to a half of the agglomerate radius, measured from the lowest point of such agglomerate, as illustrated in Fig. 1(a). This agglomerate was then set at an initial velocity for all primary particles before falling down to collide with the rigid surface, as shown in Figs. 2(a) and 2(b). The gravity is set to 9.81 m/s. We ran a series of simulations by systematically varying the cohesive stress σ_c in a range [4.0, 74.0] kN/m^2, the liquid viscosity in a range [1.0, 3000.0] mPa s, and the range of the impact velocity v_0 [0.3, 5.0] m/s. The interparticle friction coefficient is set to 0.5. All the other system parameters are shown in Table I.

III. TENSILE STRENGTH

In order to analyze the tensile stress of a viscocohesive agglomerate impacting a rigid plate, we consider the normal stresses σ_{xx} and σ_{yy} that have the direction perpendicular to the planes xz and yz, respectively, as shown in Fig. 1(b), where σ_{xx} and σ_{yy} are observed from the stress tensor by considering the tensile forces that have the direction perpendicular to the impact direction of the agglomerate.

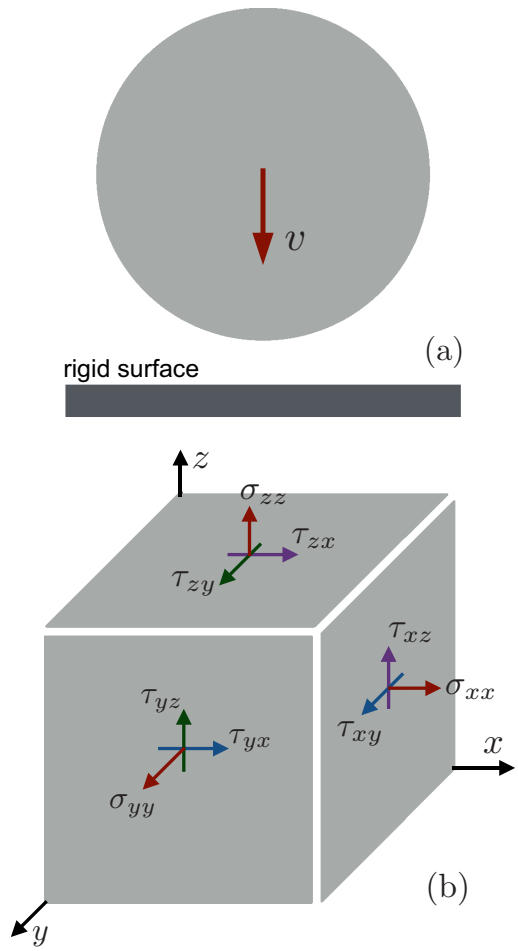

FIG. 1. (a) Schematic drawing of the impact model of a single agglomerate. (b) Schematic representation of the different components of the stress tensor in different directions and sides.

$$\sigma_{ii} = \frac{1}{V_a}\sum_{k=1}^{N_b} f_i^k \ell_i^k = n_b \langle f_i^k \ell_i^k \rangle_k, \tag{1}$$

TABLE I. Main simulation parameters.

Parameter	Symbol	Value	Unit
Smallest particle diameter	$d_{\min}$	600	μm
Density of particles	ρ	2600	kg m^{-3}
Number of particles	N_p	31 470	
Friction coefficient	μ	0.5	
Normal stiffness	k_n	10^6	N/m
Tangential stiffness	k_t	8×10^5	N/m
Normal damping	γ_n	0.5	Ns/m
Tangential damping	γ_t	0.5	Ns/m
Contact angle	θ	0	deg.
Liquid viscosity	η	[1.0, 3000]	mPa s
Cohesive stress	σ_c	[4.0, 74.0]	kN/m^2
Impact velocity	v_0	[0.3, 5.0]	m/s
Time step	Δt	2×10^{-8}	s

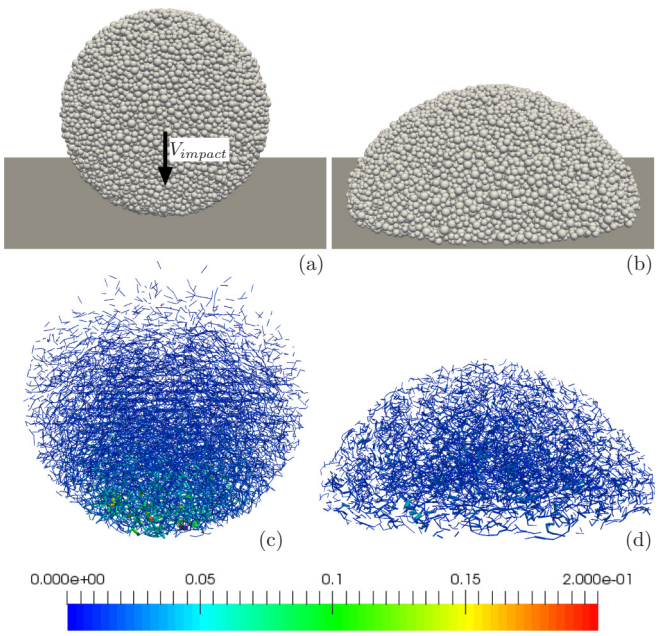

FIG. 2. Snapshots represent the geometries of a single wet agglomerate composed of spherical particles impacting a rigid plane at the early-stage impact (a) and during the deformation (b), and the distribution of the tensile forces in these two different stages (c,d). The line thickness is proportional to the tensile forces between near-neighboring particles.

where i denotes the x or y direction, V_a is the volume of aggregate at the current computational step, N_b is the number of capillary bridges having the tensile forces f_x or f_y, f_i^k and l_i^k are the i components of the force vector and branch vector of capillary bridge k, respectively, and $n_b = N_b/V_a$ is the number density of the capillary bridges. The symbol $\langle \cdots \rangle_k$ is averaging over all contacts k in the volume. The tensile stress σ_t of the agglomerate is defined as an average value of σ_{xx} and σ_{yy}, as given:

$$\sigma_t = \frac{\sigma_{xx} + \sigma_{yy}}{2}. \tag{2}$$

Figure 3 shows the evolution of the tensile stress σ_t as a function of the particle movement $D_p = v_0 \times t/\langle d \rangle$ for different values of the initial impact velocity v_0 and as a given value of the cohesive stress $\sigma_c = 46.4$ kN/m^2 and the liquid viscosity $\eta = 1000$ mPa s, where t is the impact time and $\langle d \rangle$ denotes the mean particle diameter. As we can see, the tensile stress of all agglomerates remains at a constant value in the equilibrium state (before the occurring impact). This stress then increases immediately when the agglomerate starts colliding with the rigid surface and reaches the peak that increases proportionally to the impact speed v_0 of agglomerates. It is also interesting to see that the peak of the tensile stress appears a short period of time after the collision. This may be explained by the delay of the relative movement between primary particles and the extension behavior of the capillary contacts. This property of the tensile stress is really different as compared to the compressive stress that reaches a peak at the beginning of the impact process. After reaching a peak, the tensile stress σ_t decreases smoothly due to losing the impact

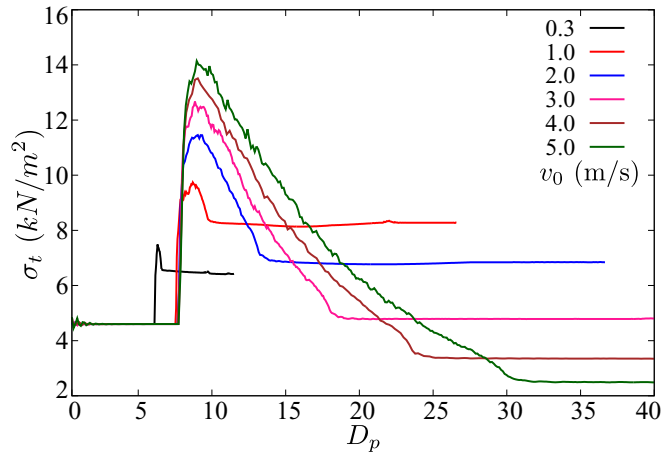

FIG. 3. Evolution of the tensile stress σ_t as a function of the particle movement D_p for different values of the impact velocity v_0.

energy; then the agglomerate reaches the stable state with the stress that decreases almost proportionally to the impact velocity.

Similar to the impact speed, the liquid properties characterized by the cohesive stress $\sigma_c = \gamma_s/\langle d \rangle$ and the liquid viscosity between primary particles also have strong influences on the tensile stress of viscocohesive agglomerates. Figures 4 and 5 display the evolution of the tensile stress σ_t as a function of the particle movement D_p for different values of the cohesive stress σ_c and the liquid viscosity η for a given value of the impact velocity. It is remarkable that the tensile stress σ_t of the viscocohesive agglomerate increases proportionally to the cohesive stress σ_c before colliding, during impacting, and in the deposition stage. These observations are also presented in Fig. 5 for different values of η.

In order to show the effects of different system parameters on the tensile stress of the viscocohesive agglomerate, we defined the tensile strength of such agglomerate. The tensile strength is obtained by normalizing the peak of σ_t with the cohesive stress σ_c of capillary bonds. Figure 6 shows all the data points of the normalized tensile strength σ_t^p/σ_c as a

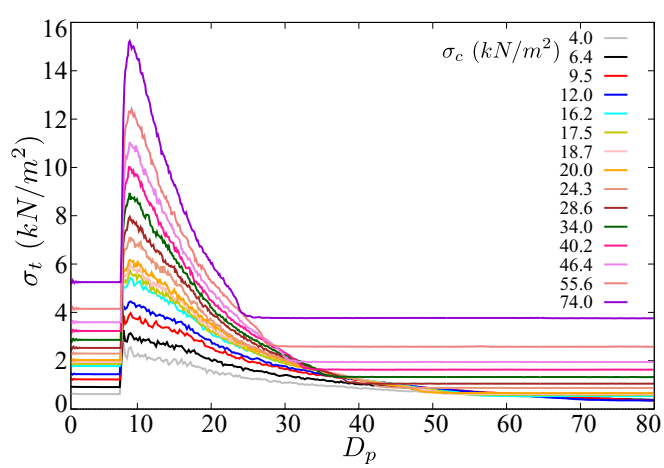

FIG. 4. Evolution of the tensile stress σ_t as a function of the particle movement D_p for different values of the cohesive stress σ_c of primary particles.

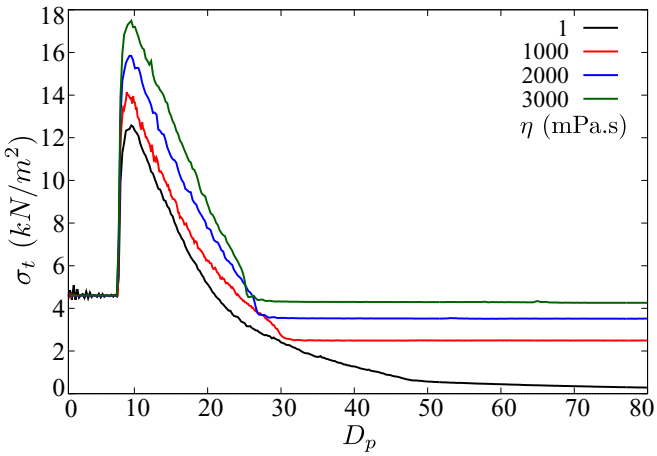

FIG. 5. Evolution of the tensile stress σ_t as a function of the particle movement D_p for different values of the liquid viscosity η.

function of the impact velocity v_i, where v_i is obtained when the lowest primary particles start touching the rigid surface. Although the impact velocity v_i is the same for each group of v_0 of the simulations, the data points are plotted separately for improving visibility. We see that the tensile strength increases proportionally to the impact speed, the cohesive stress, and the liquid viscosity η. Remarkably, the rate of these increases is almost the same order of magnitude with increasing the liquid properties. This tendency leads one to conjecture that the tensile strength of wet agglomerates is fundamentally governed by a scaling parameter that combines all key parameters including the liquid properties and the impact rate.

IV. SCALING BEHAVIOR

In the case of wet particles agglomerates impacting a rigid surface, there are three different stresses exerted on the particles including the inertial stress σ_i, the cohesive stress σ_c, and the viscous stress σ_v. The inertial stress $\sigma_i \sim \rho\langle d\rangle^2\dot{\gamma}^2$ is the stress that appears due to the collective motions of the particles as a consequence of impacting the plane, where ρ is the particle density [17,19,21,28–31]. The cohesive stress $\sigma_c \sim \gamma_s/\langle d\rangle$ and the viscous stress $\sigma_v \sim \eta\dot{\gamma}$ are induced from the capillary bonds between primary particles [17–20]. In order to define a dimensionless impact number that combines the surface tension, the viscosity of the interstitial liquid, and the impact rate $\dot{\gamma}$, we consider the linear combination of the inertial stress σ_i and the viscous stress σ_v with a weighting factor α (as given $\sigma_i + \alpha\sigma_v$) due to the same footing between them. This combination is dependent on the impact speed of the wet agglomerate.

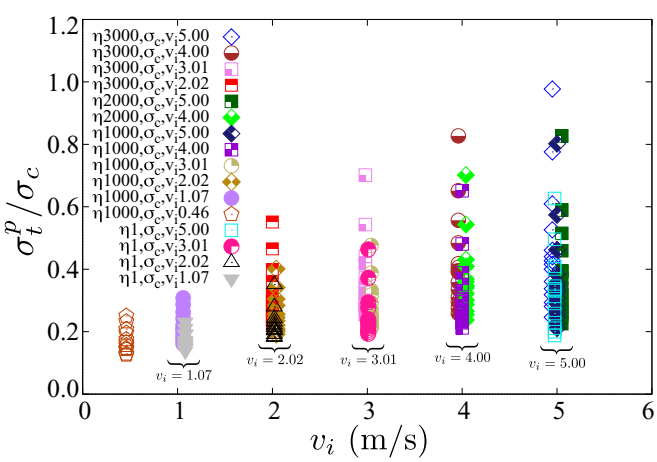

FIG. 6. The normalized tensile strength σ_t^p/σ_c as a function of the impact speed v_i. Each symbol point and its color correspond to the controlled parameters that are varied with their ranges of values; all other system parameters are kept constant.

As inertial number ($I \equiv \sqrt{\sigma_i/\sigma_p}$) in the pressure-controlled conditions shearing flows of granular materials [19,20,28,29,32–34], where σ_p is the confining pressure as external stress is exerted on the particles, the dimensionless impact number I_n in this current work is defined as a ratio of the stress combination ($\sigma_i + \alpha\sigma_v$) that is dependent on the impact rate and the cohesive stress σ_c that is independent on the impact speed of the agglomerate:

$$I_n = \sqrt{\frac{\sigma_i + \alpha\sigma_v}{\sigma_c}} = \sqrt{\frac{\sigma_i/\sigma_p + \alpha\sigma_v/\sigma_p}{\sigma_c/\sigma_p}}, \tag{3}$$

implying

$$I_n = I\sqrt{\frac{1 + \alpha/\mathrm{St}}{\xi}}, \tag{4}$$

where St is the Stokes number, defined as the ratio of the inertial stress σ_i and the viscous stress σ_v [20,25,26], and ξ is the cohesion number, defined as the ratio of σ_c and σ_p [17,18,27].

Furthermore, in the case of the confining pressure σ_p is the gravity of the primary particles, which is small as compared to the cohesive and viscous stress between particles, the inertial number I is replaced by

$$I = \sqrt{\frac{\sigma_i}{\sigma_p}} = \sqrt{\frac{\sigma_i}{\sigma_v} \times \frac{\sigma_v}{\sigma_c} \times \frac{\sigma_c}{\sigma_p}} = \sqrt{\mathrm{St} \times \mathrm{Ca} \times \xi}, \tag{5}$$

where Ca is the capillary number, defined as a ratio of the viscous stress σ_v and the cohesive stress σ_c exerts on each particle [8,19]. By integrating the combination of Eqs. (4) and (5), we get the dimensionless impact number I_n:

$$I_n = \sqrt{\mathrm{Ca}(\mathrm{St} + \alpha)}. \tag{6}$$

Hence, the tensile strength of a wet particle agglomerate impacting a rigid plane may be described as a function of this dimensionless impact number if choosing an appropriate value of the weighting factor α.

Figures 7 and 8 show the tensile strength σ_t^p/σ_c of a wet particle agglomerate impacting a flat surface as a function of the dimensionless impact number in linear-linear and log-log scales for broad ranges of values of key parameters including σ_c, η, and $\dot{\gamma}$ by setting $\alpha = 0.113$. As we can see, all the data points of σ_t^p/σ_c nicely collapse on a master curve as a function of I_n incorporating the capillary number Ca and Stokes number St (obtained from the liquid-vapor surface tension, the liquid viscosity, and the impact rate of agglomerate). This scaling thus provides the evidence that it is possible to unify the description of the cohesive and viscous stresses and the impact speed of wet granular materials in the case of a wet

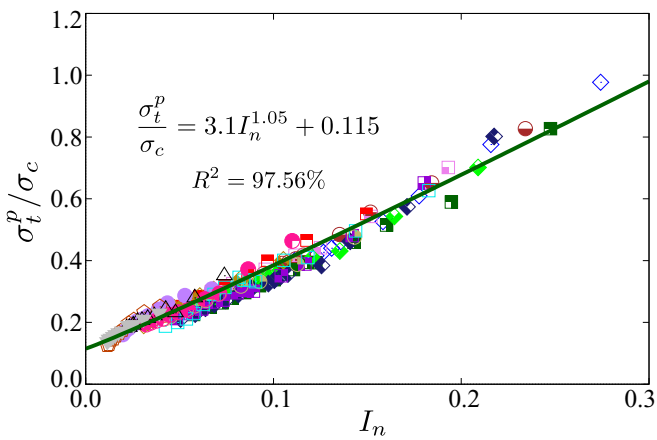

FIG. 7. Normalized tensile strength σ_t^p/σ_c as a linear function of the dimensionless impact number I_n defined by Eq. (6) by setting $\alpha = 0.113$ for all of the system parameters. The symbols and their colors are the same as Fig. 6. The solid line is the plot of Eq. (7).

agglomerate impacting a rigid plane. All the data points of the tensile strength are well fitted by the power-law functional form as follows:

$$\frac{\sigma_t^p}{\sigma_c} = A_t I_n^{\beta} + B_t, \tag{7}$$

with $A_t = 3.1$ and $B_t = 11.5 \times 10^{-2}$ the prefactors, and $\beta = 1.05$ the power of I_n. The fitting functional form confirms the dependence of different stresses in particle interactions characterized by the capillary number Ca and Stokes number St on the tensile strength of wet particle agglomerates impacting a flat surface. The correlation between all data points and the fitting form is strongly supported by a high value of the coefficient of determination $R^2 = 97.56\%$.

The mechanical strength of wet particles agglomerates has been successfully modeled by using the discrete element method with the interpretation at the particle scale for fine grains [35], coarse grains [36], and the asteroid

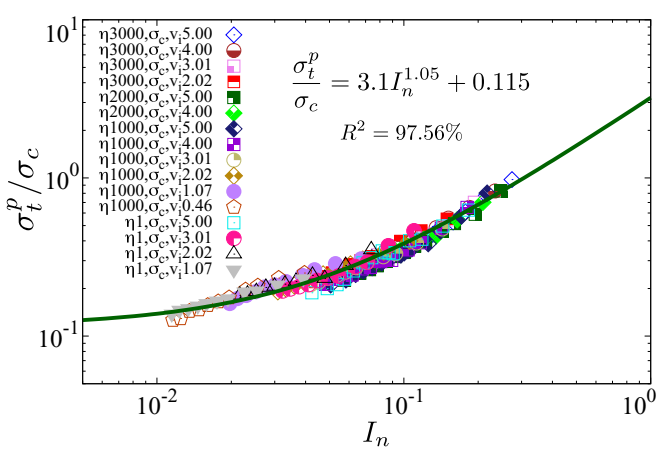

FIG. 8. Normalized tensile strength σ_t^p/σ_c in the log-log scale as a function of the dimensionless impact number I_n defined by Eq. (6) by setting $\alpha = 0.113$ for all of the system parameters. The symbols and their colors are the same as Fig. 6. The solid line is the plot of Eq. (7).

and solar level [37,38]. Previous investigations also indicated the effects of different parameters such as the particle size distribution [12,39] and the liquid content [12,40,41] on the compressive and tensile strength of agglomerates in different configurations. The current work follows the studies above. As a result, the observations presented in this paper are not only consistent with the previous investigations on the mechanical strength of wet particle agglomerates but also the scaling of rheology of unsaturated granular materials [17,19,20].

V. CONCLUSIONS

In this paper, we used a 3D discrete element approach with the inclusion of the capillary cohesion law characterized by the cohesive and viscous forces of the capillary bridges between primary particles to analyze the tensile strength of wet particle agglomerates, which are extracted from a cuboidal sample of a weak size polydispersity and subjected to impact on a rigid plane by systematically varying a broad range of values of the impact speed and the liquid properties. We showed that the tensile stress of such viscocohesive aggregates increases immediately when the collision with the flat surface occurs, then reaches a peak before decreasing smoothly and reaching constant stress at the deposition stage. The peak of the stress is called the tensile strength of wet agglomerates. This tensile strength is proportional to the cohesive stress and viscous stress of the liquid bridges as well as the impact rate of agglomerates. We also proposed a scaling behavior of tensile strength of such wet agglomerates with a dimensionless impact number that combines the capillary number and the Stokes number defined from different stresses exerted on particles. This scaling dimensionless parameter reveals the unified description of the natural properties of the binding liquid and the impact speed on the tensile strength of agglomerates in the case of considering the absence of the confining pressure.

As previously mentioned in the paper, the results represent the tensile stress and scaling behavior of the tensile strength of viscocohesive agglomerates which are extracted from the assembly of spherical particles by applying a spherical probe. Although the agglomerate is not created from the agglomeration process of wet primary particles in a rotating drum in which the raw properties of particles and the liquid content become more important, the impact test of the agglomerates on a flat surface considering the effects of the liquid properties and the impact speed also reflects the real existence of such agglomerates during impacting with storage walls, intruders, and other agglomerates. Thus, the impact test of agglomerates on a rigid surface is a simple way to understand the underlying tensile strength of wet granules. Therefore, we are proposing experimental investigations that allow for the validation of the numerical results.

ACKNOWLEDGMENTS

The author gratefully acknowledges the support of the High-Performance Computing Platform MESO@LR for running some of the simulations. The author also acknowledges Dr. Trung-Kien Nguyen for his helpful discussions.

The author declares that there are no conflicts of interest.

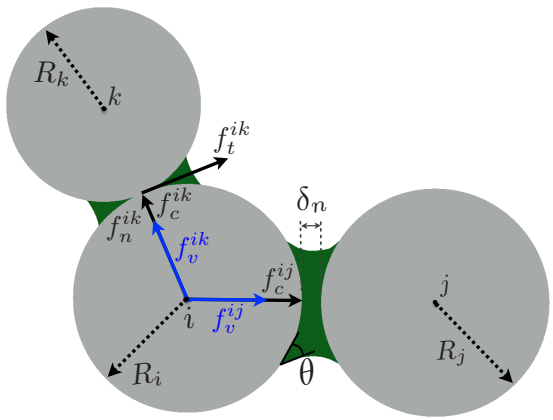

FIG. 9. Schematic drawing representation of all the forces exerted on particle i during noncontact with particle j and contact with particle k.

APPENDIX: NUMERICAL METHOD

The numerical modelings are employed by using the cFGd-3D++ code that was a private code program, initially developed by Patrick Mutabaruka; the author then developed this coding program in order to perform the current simulations. The code also has been extensively used in the simulations of granular media based on the molecular dynamics approach, with the available implementation of the solid-liquid interaction [6,12,17–20,42–44]. This discrete element method (DEM) has been used to simulate the granular materials over the last few decades [45–47]. In DEM, the particles are assumed to be rigid with the requirements of a large repulsive stiffness and a high time resolution. A particle interacts with its others via the local contact force laws [47–49]. The contact forces between particles are expressed as a function of their relative displacements. The relative displacements are computed by using the stepwise resolution of the Newton second law [47,50]. Due to the presence of the liquid bridges between particles, the cohesive and viscous forces are also implemented in each particle interaction [12,19]. The equation of motion of a particle i with its radius R_i is described under the action of all the forces involving the normal contact forces, the tangential contact forces, and the cohesive and viscous forces, as shown in Fig. 9 [12,20,51]:

$$m_\mathrm{i}\frac{d^2\mathbf{r}_\mathrm{i}}{dt^2} = \sum\left(f^{ij}\mathbf{n}^{ij} + f^{ik}\mathbf{n}^{ik} + f_\mathrm{t}^{ik}\mathbf{t}^{ik}\right) + m_i\mathbf{g},$$
$$\mathbf{I}_\mathrm{i}\frac{d\boldsymbol{\omega}_\mathrm{i}}{dt} = \sum f_\mathrm{t}^{ik}\mathbf{c}^{ik}\times\mathbf{t}^{ik}, \tag{A1}$$

where j and k are the neighboring particles, in noncontacting and contacting with particle i, respectively. $f^{ij} = f_\mathrm{c}^{ij} + f_\mathrm{v}^{ij}$ and $f^{ik} = f_\mathrm{n}^{ik} + f_\mathrm{c}^{ik} + f_\mathrm{v}^{ik}$ denote the normal forces exerted on the particle i from noncontacting with particle j and contacting with particle k, where f_n^{ik}, $f_\mathrm{c}^{ij(ik)}$, and $f_\mathrm{v}^{ij(ik)}$ are the normal contact force, the capillary cohesion forces, and the viscous forces. m_i, $\mathbf{r}_\mathrm{i}$, and $\mathbf{I}_\mathrm{i}$ are the mass, position, and inertia matrix vector of particle i. $\boldsymbol{\omega}_i$ is the rotation vector of the particle i, and $\mathbf{g}$ denotes the gravitational acceleration vector. $\mathbf{n}^{ij(ik)}$ is the unit vector that is perpendicular to the contact plane between the particles i and $j(k)$ and pointing from $j(k)$ to i. $\mathbf{t}^{ik}$ denotes the unit vector in the contact plane and pointing in the direction opposite to the relative tangential displacement between particle i and k. $\mathbf{c}^{ik}$ is the vector pointing from the center of particle i to the contact point with particle k. $f_\mathrm{n}^{ik} = f_\mathrm{n}^e + f_\mathrm{n}^d$ is the normal contact force between particle i and particle k, where $f_\mathrm{n}^e = k_\mathrm{n}\delta_\mathrm{n}$ denotes the normal elastic force, k_n and δ_n are the normal stiffness and the normal displacement at the contact point between two particles, respectively. $f_\mathrm{n}^d = \gamma_\mathrm{n}\dot{\delta}_\mathrm{n}$ is the normal damping force that depends on the normal damping parameter γ_n and the relative normal velocity $\dot{\delta}_\mathrm{n}$ [47,52].

The tangential force ($f_\mathrm{t}^{ik} = -\min\{(k_\mathrm{t}\delta_\mathrm{t} + \gamma_\mathrm{t}\dot{\delta}_\mathrm{t}), \mu f_\mathrm{nc}\}$) is defined as the minimum value of the sum of the tangential-elastic force $f_\mathrm{t}^e = k_\mathrm{t}\delta_\mathrm{t}$ and the tangential-damping force $f_\mathrm{t}^d = \gamma_\mathrm{t}\dot{\delta}_\mathrm{t}$ as compared to the threshold of the frictional force μf_nc according to the Coulomb friction law, where k_t and δ_t denote the tangential stiffness and tangential displacement of particle i, respectively, and γ_t and $\dot{\delta}_\mathrm{t}$ are the tangential damping parameter and the relative tangential velocity. μ is the interparticle friction coefficient [47,53,54].

For the consideration of the presence of the interstitial liquid in granular media, the liquid is assumed to be distributed homogeneously inside agglomerates as in the pendular state [13,14,16–18]. In this pendular regime, the liquid is assumed to be in the form of the capillary bridges [12,51], considered for noncontact between particle i and j as a common case of the capillary bonds. The capillary bridges commonly induce the capillary attraction forces f_c and the lubrication forces f_v. Upon the collision of wet particle agglomerates on a flat surface, the capillary bonds may be broken and re-formed as a consequence of insufficient time for evaporating or draining the liquid.

The cohesion force f_c between two spherical particles depends on the liquid volume V_b of the capillary bridge, the liquid-vapor surface tension γ_s, and the solid-liquid-gas contact angle θ between them. In these simulations, the particles are assumed to be perfectly wetted ($\theta = 0$), and the capillary cohesion force is the approximate solution of the Laplace-Young equation, as follows [42,55,56]:

$$f_\mathrm{c} = \begin{cases} -\kappa R, & \text{for } \delta_n < 0 \\ -\kappa R e^{-\delta_n/\lambda}, & \text{for } 0 \leqslant \delta_\mathrm{n} \leqslant \delta_\mathrm{n}^{\max} \\ 0, & \text{for } \delta_\mathrm{n} > \delta_n^{\max}. \end{cases} \tag{A2}$$

$R = \sqrt{R_\mathrm{i}R_\mathrm{j}}$ denotes the geometrical mean radius of two spherical particles i and j. $\kappa = 2\pi\gamma_s\cos\theta$ denotes the capillary attraction force prefactor. This cohesion force showed excellent agreement with previous experimental results on the cohesion of wet granular materials [55]. $\delta_\mathrm{n}^{\max}$ is the rupture distance (debonding distance), as given by [13]

$$\delta_\mathrm{n}^{\max} = \left(1 + \frac{\theta}{2}\right)V_\mathrm{b}^{1/3}. \tag{A3}$$

λ is the characteristic length that is considered as the falloff of the capillary cohesion force in Eq. (A2),

$$\lambda = ch(r)\left(\frac{V_\mathrm{b}}{R'}\right)^{1/2}, \tag{A4}$$

where $R' = 2R_\mathrm{i}R_\mathrm{j}/(R_\mathrm{i} + R_\mathrm{j})$ is the harmonic mean radius, $r = \max\{R_\mathrm{i}/R_\mathrm{j}; R_\mathrm{j}/R_\mathrm{i}\}$ is the ratio of two particle diameters i and j in the contact, $h(r) = r^{-1/2}$, and $c \simeq 0.9$ [14,55,57].

The liquid viscous force f_v is due to the lubrication effects of the capillary bridges and is given here by the following expression [11,20,58]:

$$f_v = \begin{cases} \frac{3}{2}\pi R^2 \eta \frac{v_n}{\delta_0}, & \text{for } \delta_n \leqslant 0 \\ \frac{3}{2}\pi R^2 \eta \frac{v_n}{\delta_n + \delta_0}, & \text{for } 0 < \delta_n \leqslant \delta_n^{\max} \\ 0, & \text{for } \delta_n > \delta_n^{\max}, \end{cases} \tag{A5}$$

where η is the liquid viscosity of the capillary bonds, and v_n denotes the relative velocity between two spherical particles i and j during the contact; this velocity is assumed to be negative when the separation distance δ_n tends to increase. δ_0 is the characteristic length of the particle roughness, assumed to equal $\delta_0 = 5.0 \times 10^{-4} d_{\min}$ in this current work, with $d_{\min}$ the smallest particle diameter.

[1] S. H. Chien, G. Carmona, L. I. Prochnow, and E. R. Austin, J. Environ. Qual. **32**, 1911 (2003).
[2] A. Barkouti, E. Rondet, M. Delalonde, and T. Ruiz, J. Food Eng. **111**, 234 (2012).
[3] A. Nosrati, J. Addai-Mensah, and D. J. Robinson, Hydrometallurgy **125-126**, 90 (2012).
[4] R. Affes, J.-Y. Delenne, Y. Monerie, F. Radjai, and V. Topin, Eur. Phys. J. E **35**, 117 (2012).
[5] P. Suresh, I. Sreedhar, R. Vaidhiswaran, and A. Venugopal, Chem. Eng. J. **328**, 785 (2017).
[6] T.-T. Vo, S. Nezamabadi, P. Mutabaruka, J.-Y. Delenne, E. Izard, R. Pellenq, and F. Radjai, Eur. Phys. J. E **42**, 127 (2019).
[7] G. Lian, C. Thornton, and M. J. Adams, Chem. Eng. Sci. **53**, 3381 (1998).
[8] S. M. Iveson, J. D. Litster, K. Hapgood, and B. J. Ennis, Powder Technol. **117**, 3 (2001).
[9] K. Kafui and C. Thornton, Powder Technol. **109**, 113 (2000).
[10] C. Thornton, M. T. Ciomocos, and M. J. Adams, Powder Technol. **140**, 258 (2004).
[11] G. Lefebvre and P. Jop, Phys. Rev. E **88**, 032205 (2013).
[12] T.-T. Vo, P. Mutabaruka, S. Nezamabadi, J.-Y. Delenne, E. Izard, R. Pellenq, and F. Radjai, Mech. Res. Commun. **92**, 1 (2018).
[13] G. Lian, C. Thornton, and M. Adams, J. Colloid Interface Sci. **161**, 138 (1993).
[14] V. Richefeu, Moulay Said El Youssoufi, and F. Radjai, Phys. Rev. E **73**, 051304 (2006).
[15] T. T. Vo, Thesis, Université de Montpellier, 2019.
[16] M. Scheel, R. Seemann, M. Brinkmann, M. D. Michiel, A. Sheppard, and S. Herminghaus, J. Phys.: Condens. Matter **20**, 494236 (2008).
[17] T.-T. Vo, P. Mutabaruka, S. Nezamabadi, J.-Y. Delenne, and F. Radjai, Phys. Rev. E **101**, 032906 (2020).
[18] T.-T. Vo, Comput. Part. Mech. **7** (2020), doi: 10.1007/s40571-020-00357-y.
[19] T.-T. Vo, S. Nezamabadi, P. Mutabaruka, J.-Y. Delenne, and F. Radjai, Nat. Commun. **11**, 1476 (2020).
[20] T.-T. Vo, J. Rheol. **64**, 1133 (2020).
[21] S. Khamseh, J.-N. Roux, and F. Chevoir, Phys. Rev. E **92**, 022201 (2015).
[22] S. Roy, S. Luding, and T. Weinhart, New J. Phys. **19**, 043014 (2017).
[23] M. Badetti, A. Fall, D. Hautemayou, F. Chevoir, P. Aimedieu, S. Rodts, and J.-N. Roux, J. Rheol. **62**, 1175 (2018).
[24] F. Boyer, E. Guazzelli, and O. Pouliquen, Phys. Rev. Lett. **107**, 188301 (2011).
[25] M. Trulsson, B. Andreotti, and P. Claudin, Phys. Rev. Lett. **109**, 118305 (2012).
[26] L. Amarsid, J.-Y. Delenne, P. Mutabaruka, Y. Monerie, F. Perales, and F. Radjai, Phys. Rev. E **96**, 012901 (2017).
[27] N. Berger, E. Azéma, J.-F. Douce, and F. Radjai, Europhys. Lett. **112**, 64004 (2015).
[28] GDR-MiDi, Eur. Phys. J. E **14**, 341 (2004).
[29] F. da Cruz, S. Emam, M. Prochnow, J.-N. Roux, and F. Chevoir, Phys. Rev. E **72**, 021309 (2005).
[30] P. G. Rognon, J.-N. Roux, D. Wolf, M. Naaim, and F. Chevoir, Europhys. Lett. **74**, 644 (2006).
[31] P. Rognon, J.-N. Roux, M. Naaim, and F. Chevoir, J. Fluid Mech. **596**, 21 (2008).
[32] P. Jop, Y.Forterre, and O.Pouliquen, Nature (London) **441**, 727 (2006).
[33] O. Pouliquen, C. Cassar, P. Jop, Y. Forterre, and M. Nicolas, J. Stat. Mech. (2006) P07020.
[34] Y. Forterre and O. Pouliquen, Annu. Rev. Fluid Mech. **40**, 1 (2008).
[35] Z. Tong, R. Yang, A. Yu, S. Adi, and H. Chan, Powder Technol. **196**, 213 (2009).
[36] Q. Zheng and A. Yu, Powder Technol. **286**, 361 (2015).
[37] E. Azéma, P. Sánchez, and D. J. Scheeres, Phys. Rev. E **98**, 030901(R) (2018).
[38] M. Tatsuuma, A. Kataoka, and H. Tanaka, Astrophys. J. **874**, 159 (2019).
[39] A. Spettl, M. Dosta, S. Antonyuk, S. Heinrich, and V. Schmidt, Adv. Powder Technol. **26**, 1021 (2015), special issue of the 7thWorld Congress on Particle Technology.
[40] J. Horabik, J. Wiacek, P. Parafiniuk, M. Stasiak, M. Banda, and M. Molenda, Biosyst. Eng. **183**, 95 (2019).
[41] X. Frank, F. Radjaï, S. Nezamabadi, and J.-Y. Delenne, Phys. Rev. E **102**, 022906 (2020).
[42] T.-T. Vo, P. Mutabaruka, J-Y. Delenne, S. Nezamabadi, and F. Radjai, EPJ Web Conf. **140**, 08021 (2017).
[43] P. Mutabaruka, M. Taiebat, Roland J.-M. Pellenq, and F. Radjai, Phys. Rev. E **100**, 042906 (2019).
[44] T.-T. Vo and T. Nguyen-Thoi, Eur. Phys. J. E **43**, 052901 (2020).
[45] P. A. Cundall and O. D. L. Strack, Géotechnique **29**, 47 (1979).
[46] C. Thornton, Powder Technol. **109**, 179 (1999).
[47] F. Radjai and F. Dubois, *Discrete-Element Modeling of Granular Materials* (Wiley-Iste, New York, 2011).
[48] H. J. Herrmann and S. Luding, Continuum Mech. Thermodyn. **10**, 189 (1998).
[49] S. Luding, in *Physics of Dry Granular Media—NATO ASI Series E350*, edited by H. J. Herrmann, J.-P. Hovi, and S. Luding (Kluwer Academic, Dordrecht, 1998), p. 285.
[50] M. P. Allen and D. J. Tildesley, *Computer Simulation of Liquids* (Oxford University Press, Oxford, 1987).

[51] V. Richefeu, M. S. El Youssoufi, R. Peyroux, and F. Radjai, Int. J. Numer. Anal. Methods Geomech. **32**, 1365 (2007).
[52] J. Duran, A. Reisinger, and P. de Gennes, *Sands, Powders, and Grains: An Introduction to the Physics of Granular Materials*, Partially Ordered Systems (Springer, New York, 1999).
[53] J. Schäfer, S. Dippel, and D. E. Wolf, J. Phys. I **6**, 5 (1996).
[54] S. Dippel, G. G. Batrouni, and D. E. Wolf, Phys. Rev. E **56**, 3645 (1997).
[55] V. Richefeu, F. Radjai, and M. S. E. Youssoufi, Eur. Phys. J. E **21**, 359 (2007).
[56] T. Mikami, H. Kamiya, and M. Horio, Chem. Eng. Sci. **53**, 1927 (1998).
[57] F. Radjaï and V. Richefeu, Philos. Trans. R. Soc., A **367**, 5123 (2009).
[58] J. Happel and H. Brenner, *Low Reynolds Number Hydrodynamics* (Martinus Nijhoff, The Hague, the Netherlands, 1983).